




## Article

# Dependence of Power Characteristics on Savonius Rotor Segmentation

Krzysztof Doerffer <sup>1</sup>, Janusz Telega <sup>2,\*</sup>, Piotr Doerffer <sup>2</sup>, Paulina Hercel <sup>2</sup> and Andrzej Tomporowski <sup>3</sup>

<sup>1</sup> Department of Manufacturing and Production Engineering, Faculty of Mechanical Engineering, Gdansk University of Technology, Gabriela Narutowicza 11/12, 80-233 Gdańsk, Poland; krzysztof.doerffer@pg.edu.pl

<sup>2</sup> Institute of Fluid Flow Machinery, Polish Academy of Sciences, Fiszerka 14, 80-231 Gdańsk, Poland; doerffer@imp.gda.pl (P.D.); phercel@imp.gda.pl (P.H.)

<sup>3</sup> Faculty of Mechanical Engineering, UTP University of Science and Technology, Kaliskiego 7, 85-796 Bydgoszcz, Poland; a.tomporowski@utp.edu.pl

\* Correspondence: januszt@imp.gda.pl; Tel.: +48-697-626-179

**Abstract:** Savonius rotors are large and heavy because they use drag force for propulsion. This leads to a larger investment in comparison to horizontal axis wind turbine (HAWT) rotors using lift forces. A simple construction of the Savonius rotor is preferred to reduce the production effort. Therefore, it is proposed here to use single-segment rotors of high elongation. Nevertheless, this rotor type must be compared with a multi-segment rotor to prove that the simplification does not deteriorate the effectiveness. The number of segments affects the aerodynamic performance of the rotor, however, the results shown in the literature are inconsistent. The paper presents a new observation that the relation between the effectiveness of single- and multi-segment rotors depends on the wind velocity. A single-segment rotor becomes significantly more effective than a four-segment rotor at low wind speeds. At high wind speeds, the effectiveness of both rotors becomes similar.

**Keywords:** small wind turbines; vertical axis wind turbines (VAWT); Savonius rotor; rotor effectiveness; rotor experimental testing



**Citation:** Doerffer, K.; Telega, J.; Doerffer, P.; Hercel, P.; Tomporowski, A. Dependence of Power Characteristics on Savonius Rotor Segmentation. *Energies* **2021**, *14*, 2912. <https://doi.org/10.3390/en14102912>

Academic Editor: Davide Astolfi

Received: 18 March 2021

Accepted: 11 May 2021

Published: 18 May 2021

**Publisher's Note:** MDPI stays neutral with regard to jurisdictional claims in published maps and institutional affiliations.



**Copyright:** © 2021 by the authors. Licensee MDPI, Basel, Switzerland. This article is an open access article distributed under the terms and conditions of the Creative Commons Attribution (CC BY) license (<https://creativecommons.org/licenses/by/4.0/>).

## 1. Introduction

The scope of this paper is focused on small and micro wind turbines. In this market sector, the situation is very different from the large wind turbine market, where a single design concept has been established. In the large turbine market, the design concept has converged over several decades to a horizontal axis wind turbine (HAWT) equipped with a three-bladed rotor.

The small wind turbine market changes in a different way. The development is very rapid and significantly growing [1,2] throughout the world. A characteristic feature of the small and micro wind turbine sector is that there is no convergence of the turbine design concept to a single type. Therefore, many different turbine types are offered. It should be pointed out that there are turbines using the lift force and other turbines using the drag force. The lift force-driven turbines are the typical HAWT and VAWT of the Darrieus-type, shown in Figure 1. The existing literature on small wind turbines is very extensive and, therefore, we refer here to some works, as examples only, without exhausting the whole literature background.

The propelling blades of wind turbines using lift force move with a much higher velocity than the wind itself. The lift force depends on the blade velocity squared ( $U^2$ ), and, therefore, a small area of the blade may be used when the blade velocity is high. Hence, the blades in such wind turbines are slim (Figure 1). Nevertheless, such designs, with a high speed of rotation, leads to the possibility of rotor overspeed that may result in rotor destruction. Therefore, in the case of lift force-driven turbines, safety must be compromised

or the effectiveness must be limited and these turbines mostly are equipped with a brake. A turbine of this type must be actively stopped at high winds.

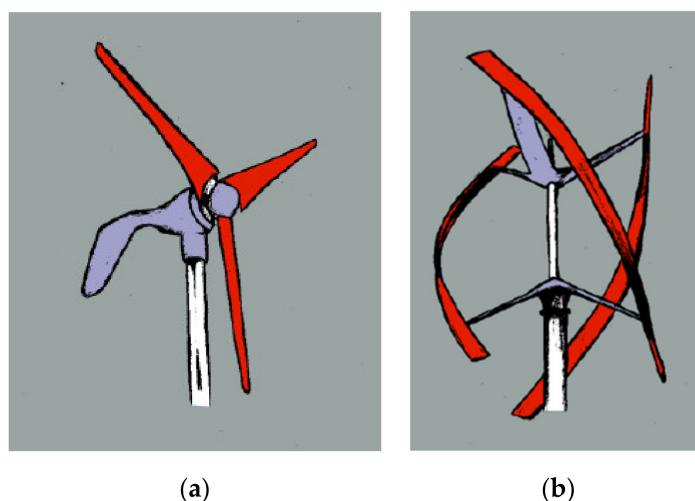


**Figure 1.** Wind turbines using lift force; (a) HAWT; (b) VAWT.

In the case of wind turbines using drag force (Figure 2), the blades are moving slower than the wind. The only way to increase the aerodynamic forces acting on the rotor is to use large blades. Therefore, it can be noticed that the rotor projection area covers nearly the whole wind stream in such wind turbines.

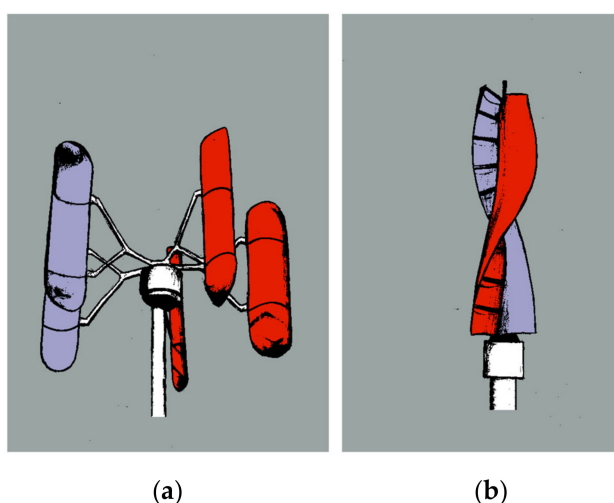


**Figure 2.** Turbines using drag force; (a) VAWT with drag elements; (b) Savonius VAWT.

It should be also mentioned that, in the case of horizontal axis wind turbines (HAWT) propulsion is delivered by the whole area being swept by the blades. This type of turbine is illustrated in Figure 1a. In the case of vertical axis wind turbines (VAWT) driven by drag force (Figure 2), the blades on one side of the rotor axis are moving against the wind, reducing the generated power. Due to this feature, the energy production by VAWT is expected to be smaller than by HAWT.

The most important feature, necessary for small-size wind turbines used in close vicinity to residential areas and people, is safety. Rotors that may overspeed should be avoided. This aspect suggests the choice of drag-driven turbines for the prosumer market (meaning the producer and consumer of energy). This is the reason why special attention in our considerations on micro wind turbines is focused on Savonius rotors.

In the drag force-driven turbines, high aerodynamic forces are induced by strong winds due to the large area covered by blades. This requires that the turbine should

have a strong base and support structure, which leads to the high weight of the wind turbine. Thus, the weight issue is a very important aspect in the development of such micro wind turbines.

All elements of the wind turbine should be considered with the objective of reducing the weight. Nonetheless, there is one element whereby the modifications may influence energy production effectiveness; this is the rotor. It seems that a straight one-segment rotor may be the simplest and most lightweight design of the Savonius turbine. Nevertheless, the question should be answered, if and how the number of segments is affecting the energy production by the rotor. In this paper, we are delivering an answer to this question. The research carried out concerns a comparison between the effectiveness of a single-segment rotors and four-segment rotors, both with identical overall dimensions, both investigated in identical experimental conditions. The measurement equipment and data reduction procedures are also identical. The answer presented here allows the selection of the most suitable rotor. The innovation presented here results is the indication that the difference between four-segment and single-segment rotors depends on the wind velocity. It is shown that the single segment rotor is more effective at low wind velocities, which is an important practical conclusion of the presented results.

## 2. Research Motivation and Objectives

The well-known, traditional rotor design was developed by Savonius and patented as early as 1926 [3]. Savonius turbine modifications have been investigated experimentally and numerically throughout the years [4–10]. The need for improvement of the effectiveness has led to numerous modifications and extensive studies of those concepts. Savonius himself proposed several variants of his rotor [3], but other researchers have contributed substantially to the development of different improvements [11–18].

Sun et al. [12] and also Shigetomi et al. [19] focused their interest on wind turbine interaction and how this may improve their effectiveness. Several concepts of the Savonius rotor were selected by Tahani et al. [13] where the rotor effectiveness was enhanced with flow directing capability. The experimental validation of the numerical simulations by Driss et al. [14] confirmed the improvement of the rotor effectiveness by the proposed blade shape modification in comparison to the reference cylindrical blade. Another popular topic of research is the periodic fluctuation of the rotor torque with a frequency resulting from the number of blades and the speed of rotation [18,20,21]. An attempt to combine and summarize the results of experimental and numerical studies has been made in a number of review papers [7–9,22].

Many authors have investigated the classical Savonius rotor obtaining the power coefficient in the range of 15–30%, focusing their attention also on rotor elongation [21,23,24].

Successful commercialization of drag-driven wind turbines will depend strongly on wind turbine cost, which is directly related to wind turbine weight and design complexity. Every component of the wind turbine should be considered for improvement in this respect. This leads to the idea of using rotors with large elongation. However, this makes the driving torque act intermittently, having two impulses per rotation [18,21]. The periodicity of the generated torque has to be taken into account in the design of the supporting structure as it increases the fatigue loads originating from wind action [25].

Helical rotors have been developed to avoid this unsteady behavior [26]. Their smooth and corrugated version has been developed and implemented (Figure 3). Such rotors have to be manufactured from composite material or plastic, which is not a cheap solution, and the durability of such materials in rotor application is limited.

A variety of rotors have been investigated as helical, segmented and with additional elements [19–23,26]. Savonius rotors are used as a single wind turbine application but also in various innovative configurations, as presented in [24,27,28].

A method for smearing the torque oscillation at the rotor axis, simpler than using helical blades, is the application of several segments in one rotor, as shown in Figure 4a. Each segment may be shifted angularly in relation to the other segments in order to divide

the torque impulses over the rotation. In the case of using rotor axial multiplication, as shown in [24] and in Figure 4c, the aspect of segmentation is not so important because rotors with high elongation may be mounted in different angular positions, giving the same effect on the torque fluctuations in the generator, as a multi-segment rotor.

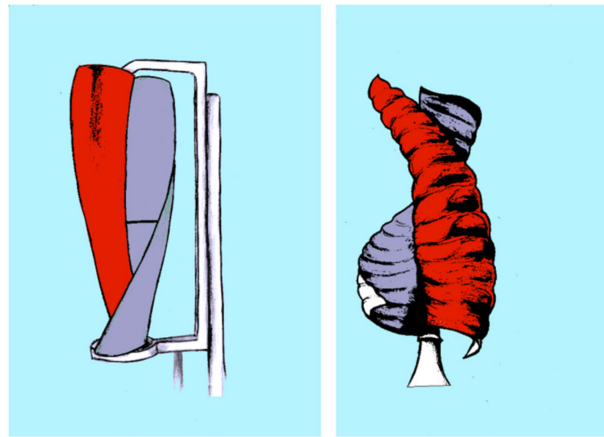


Figure 3. Helical Savonius rotors.

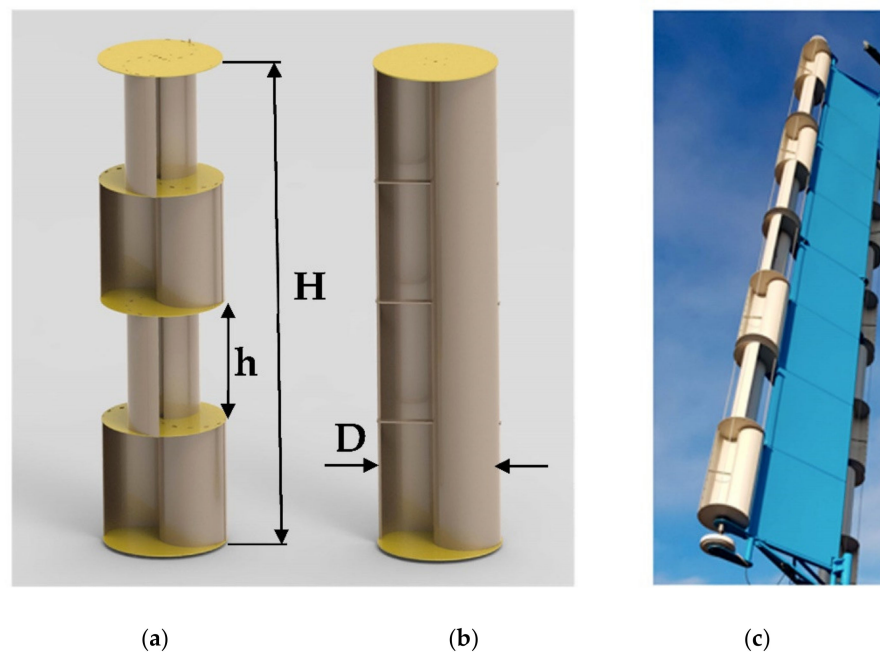


Figure 4. Segmented rotors; (a) four segments; (b) single segment; (c) multi rotor test turbine; height  $H$  and diameter  $D$  are the same for both (a,b) rotors.

An important feature of the Savonius rotor is its operational safety. This rotor does not overspeed. If the generated power cannot be used, the rotor sets higher revolutions, but they are finite without a tendency to overspeed. The rotor tip speed may become even greater than the wind speed ( $TSR > 1.0$ ). In such a case, the rotor transfers the energy into the surrounding air and acts as a rotor braking system. This important feature gives operational safety and makes such rotors attractive. Therefore, it is expected that Savonius rotors may become more popular in the prosumer market, which still includes many different wind turbine types. However, the way to success is in investment cost reduction. The introduction of very large rotor elongation may be a step in this direction.

It is easy to imagine that a multi-segment rotor is more complex to manufacture and heavier due to the inclusion of segment dividing plates. In our particular case, the

four-segment rotor weights 6 kg (Figure 4a) while the weight of a single-segment rotor is 4 kg (Figure 4b). From this point of view, a single-segment rotor is a better solution. The difference in weight of the rotor should have an effect on rotor dynamics but, in the present paper, we are considering aerodynamic characteristics at stable rotor conditions. In this case, the rotor weight has no effect on obtained results.

The advantage of a multi-segment rotor is its smoother torque distribution compared to the single-segment rotor. The experimental data from Menet [29] highlight the benefits of the multi-segment solution presenting the expected starting torque for one- and double-step rotors. The author points out that, in a two-segment design, the starting torque is never negative and never around zero, whatever the direction of the wind. Nonetheless, it is known that single-segment rotor torque also never drops to negative values; however, the minimum torque is low.

On the other hand, some researchers conclude that increasing the number of segments might reduce the power coefficient since only one segment works with at maximum performance at one time. Experimental investigations of this aspect were conducted by Jian et al. [30]. The authors obtained the value of  $c_{pmax} = 0.17$  for a single-segment rotor and 0.14 for a two-segment design. A similar result was reported by Hayashi et al. [31] who experimentally studied single-segment and three-segment rotors obtaining  $c_{pmax}$  of 0.16 and 0.12, respectively. One should also point out here that Hayashi used a very low aspect ratio of segments,  $Ar = 0.7$  and 0.22, respectively. However, a different result was obtained experimentally by Saha et al. [6] who reported an increase in the value of  $c_{pmax}$  from 0.18 for a single-segment rotor up to 0.29 for a two-segment rotor. Increasing the number of segments up to three resulted, however, in the reduction of the power coefficient to  $c_{pmax} = 0.23$ . The result for a two-segment rotor of  $c_{pmax} = 0.29$  is extremely high, but the reason for this was not explained by the authors.

Most typically the segment height is equal to one or two rotor diameters. There is not much material on the effect of this rotor aspect as it requires experimental investigations [6,30,31] or fully 3-D unsteady numerical simulations [21,23,32]. Careful numerical investigations in [23] indicate that rotor effectiveness increases with elongation (Figure 5), which was studied up to the aspect ratio 5. It is also suggested by the author that rotor elongation should not be smaller than  $H/D = 2$ .

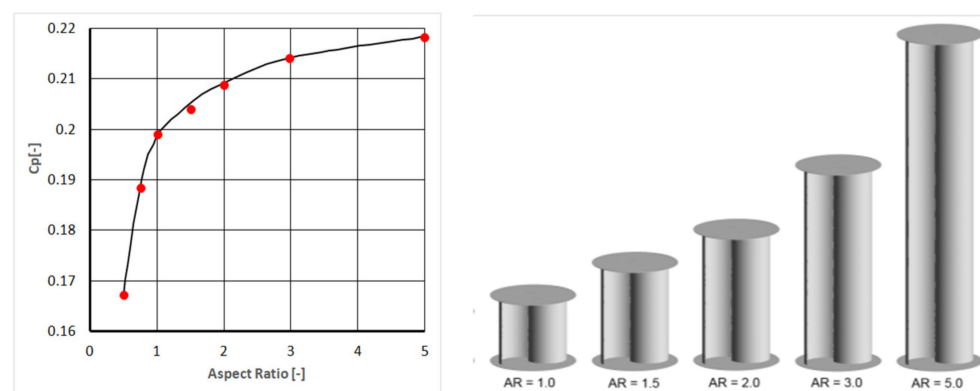


Figure 5. Two-bladed Savonius rotor aspect ratio effect [23].

The information available in the literature on the segmented rotor is contradictory. A comparison between a single-segment rotor of elongation 2 and a two-segment rotor of elongation 1 in [23] provides a similar power coefficient. This indicates that a one-segment dividing plate only is not sufficient to cause a noticeable difference. In [6] a two-segment rotor gives an extremely high maximum power coefficient, which is not fitting with the gradual increase of  $c_p$  between one- and three-segment rotors. In [21], the two rotors considered have a very small aspect ratio difference  $Ar = 0.7$  and 1.11. In this paper the rotor geometry and flow conditions are different. The material found in the literature does not allow for any unequivocal conclusions.



Therefore, our own research for particular rotor designs was carried out to provide arguments for one's own decisions to choose the rotor. We decided to use a more significant difference in the number of segments for comparison to avoid unclear effects involving one or two segments. Therefore, single- and four-segment rotors were investigated (Figure 4a,b).

The reason for reducing the number of segments is mainly to lower the manufacturing complexity and reduce the weight. Nevertheless, it should be emphasized that rotor modifications should never deteriorate the rotor's effectiveness. Therefore, the effect of rotor modifications on the aerodynamics and effectiveness should be fully verified.

Summarizing most of the information found in the literature, one can expect that increased elongation brings a positive effect on rotor effectiveness. However, this enhances the instability of the torque on the rotor axis. However, in the authors' wind turbine concept [24], the generator is driven by a line of several rotors, located one over the other (Figure 4c). They may be set with a shift of an angular position, allowing smooth distribution of torque peaks within a rotation without the necessity to use segmented rotors.

### 3. Experimental Investigations

The investigated aspect of the Savonius rotor design in this paper was, therefore, the elongation (aspect ratio) of the rotor segments. The rotors used in this experiment are shown in Figure 4a,b. They both are  $H = 1.0$  m high and  $D = 0.25$  m in diameter; the segment aspect ratio is  $Ar = 1$  and  $Ar = 4$ . One rotor consists of four segments (Figure 4a) and the other is composed of a single segment (Figure 4b) [19,28].

A special stand for rotor performance investigation was built at the IMP PAN laboratory, Gdańsk, Poland. A 2.2 kW fan, 1 m in diameter, was blowing the air stream into the test section through a flow straightener. The straightened circular stream was flowing into the compensating reservoir, converging towards the rectilinear part of the passage, the entrance to which was covered by a mesh compressing the flow and spreading the stream over the rectangular cross-section of the rectilinear passage. The test section channel, at a distance of 2.0 m, was reshaping the stream into a rectangular outlet 1.2 m high and 0.4 m wide (Figure 6). A test rotor,  $H = 1$  m high and  $D = 0.25$  m in diameter, was inserted in the outlet stream. It should be emphasized that the rotor was placed outside the test section. This is an open test section of a wind tunnel, therefore, there is no flow blocking effect as would be if the rotor was inside the test section. The rotor is located close to the channel outlet in order to avoid the stream mixing with ambient stationary air, which would also affect the core of the air stream coming from the channel.

This type of test section always induces much uncertainty as to whether such conditions may be representative of rotor behavior in the open air. Such questions imply that open-air conditions mean a steady and uniform stream of a constant velocity. This is idealistic, wishful thinking because in real open-air conditions the wind is very changeable in temporal and spatial terms. The environment is obviously essential to investigate the absolute characteristics of a rotor. We may have a large, closed test section with a relatively small turbine inside to minimize the blocking effect, as in [17,26]. One can also have an 'open test section' wind tunnel where the air stream is blown into stagnant air onto the test rotor [6,31]. The quality of the stream blown on the test rotor is very important when the objective is to compare the rotor characteristics against other types of rotors, juxtaposed with experiments performed in other labs. None of the approaches used in a wind turbine analysis reflect the conditions of a uniform and endless stream. Those closest to real conditions are the experiments of Blackwell [17] who used a very large wind tunnel, which, therefore, have become a reference database for many papers in this field.

In the case of the study presented here, we want to compare one rotor against another. For such an objective, the important issue is that both rotors are exposed to the same conditions.

The stream velocity field at the test section outlet was measured by a hot wire probe in a grid of 100 measurement points. The tests were carried out at maximum fan operating

conditions which enabled the largest non-uniformity. This section is very close to the rotor and, therefore, the air stream indicates the rotor upstream effect with a lower velocity in the central part and an increased velocity on both sides of the rotor (Figure 7a). The measurements were carried out with the rotor operating at low power conditions. The non-uniformity of the stream at the test section outlet is the same for both rotors, which is important for the present comparative study. The difference in velocity filed for both rotors at the same wind velocity is presented in Figure 7b. These differences are small, confirming the fact that both rotors are exposed to the same flow conditions.

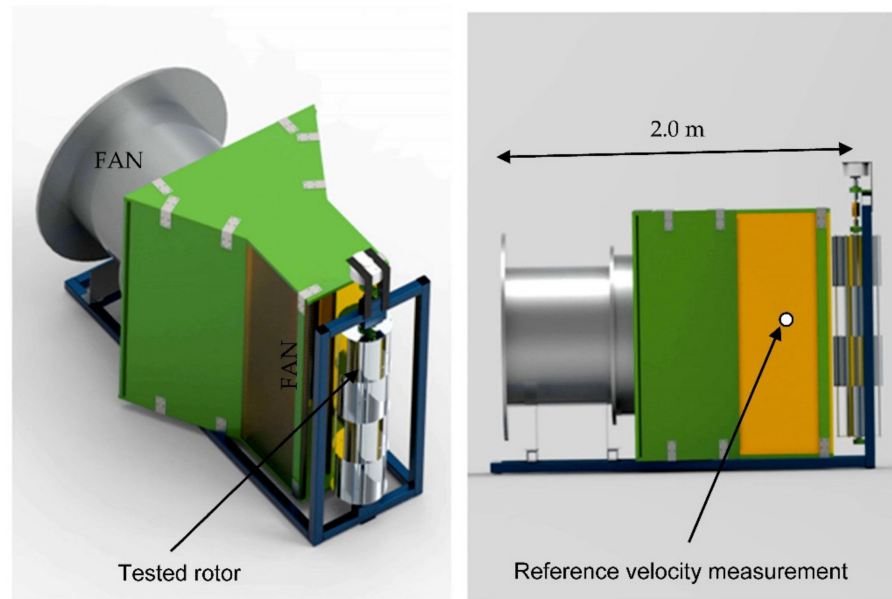


Figure 6. Experimental stand.

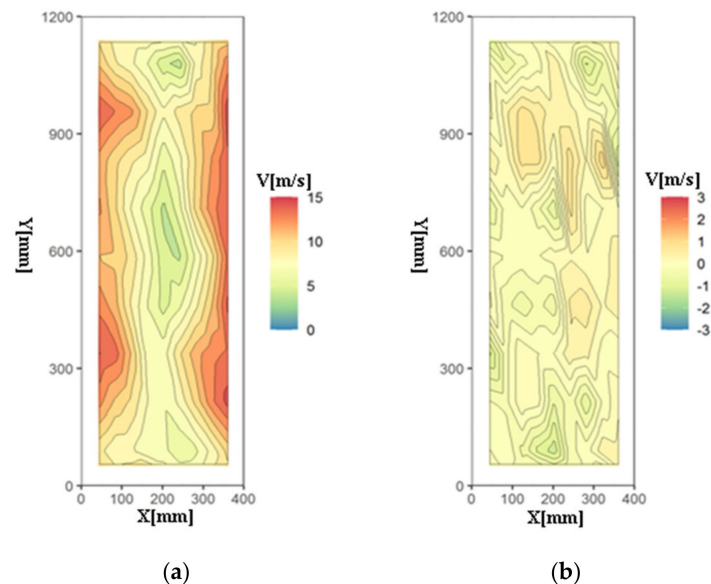


Figure 7. Velocity map; (a) with single-segment rotor; (b) difference between a single-segment and four-segment rotor.

The reference velocity for each test case was measured upstream of the outlet, inside the last constant cross-section part of the wind channel, as indicated in Figure 6. The outlet stream turbulence was measured in the middle of the outlet cross-section. The turbulence level was measured without the presence of rotors which would induce additional fluctuation.

tuations. The tests were carried out for low outlet velocity, 5.0 m/s, and for high velocity, 7.5 m/s. Measured turbulence levels were 10% and 11.5%, respectively. In this simple test section, such a level of turbulence is not surprising. Such a level of turbulence is typical for wind turbines [33,34]. Moreover, it is worth mentioning that in measured velocity fluctuations there is no trace of blade passing frequency. This means that the used flow straightener and meshes are effective.

It was necessary to measure the rotational speed of the Savonius rotor and the torque at the rotor axis to determine the rotor power output. The torque was measured by an NCTE sensor and the result was averaged over several rotations at a high sampling rate of 1 kHz (this value is sufficiently high when compared against the RPM values that are of interest in our experiment). The rotor loading was enforced by a dedicated electric generator the characteristics of which were measured at the IMP PAN laboratory. The rotational speed was measured in two ways, by sampling the generator signal and by using Hall sensors mounted on the rotor, both enabling very accurate measurements. The exact uncertainty of this measurement is described in Section 6, but it can be considered as exact when compared to other measurements. The measurements were performed in a low wind velocity range of 5 to 7.5 m/s for which stream uniformity is better than in Figure 7.

There are always numerous details to be discussed on the test section configuration and measurement system operation. In our case, the important issue is that both rotors were investigated in an identical environment and with the same measurement systems and procedures. The analysis of measurement reliability and errors is presented in Section 6 of this paper.

#### 4. Measurements and Data Analysis

The investigations were carried out to determine the power characteristics of both rotors. Each measurement session started with a selected wind velocity adjustment. At these wind conditions, the loading on the rotor was set to several values. The rotor conditions for each load value were stabilized, allowing the reading of torque ( $M$ ) and the rotation speed to be taken. The set of such measured data was used to obtain the rotor characteristics for each wind velocity case in the form of  $M = f(\text{TSR})$ .

The measured angular speed of the rotor  $\omega$  and the rotor radius allowed us to calculate the tangential velocity of the rotor outer circumference  $V_R$ . This velocity would always be normalized with the reference wind velocity to provide the so-called ‘tip speed ratio’ (1):

$$\text{TSR} = V_R / V_{\text{WIND}} \quad (1)$$

The TSR was used in the plots as abscissa, as in most of the publications. The measured torque  $M$  [Nm] was used as the ordinate. Six wind velocity cases were measured for both rotors. These were:  $V_{\text{WIND}} = 5.0; 5.5; 6.0; 6.5; 7.0$  and  $7.5$  m/s, which mean the Reynolds number ( $Re$ ) was based on rotor diameter in a range from 150,000 to 250,000. The torque was measured between the rotor and the generator which was controlling the load of the rotor. This means that the torque taken by the bearings was reducing the torque provided by the rotor. We assumed that this power consumed by the bearing was the same for both rotors and did not affect the main objective of our investigation.

In order to gain confidence in the experimental approach presented here, one should refer to dimensionless coefficients. In this case, the torque coefficient (2) needs to be compared to other studies shown in the literature. It is a coefficient that provides the relation between the measured torque value normalised by the reference torque (3). This reference value is the product of the wind dynamic head acting over rotor area  $A$  and the rotor radius. This is presented by the expressions shown below:

$$c_m = M / M_0 \quad (2)$$

$$M_0 = F_0 R = \left( \frac{\rho}{2} V_w^2 A \right) R \quad (3)$$



All the measurement points for the single-segment rotor are presented in Figure 8.

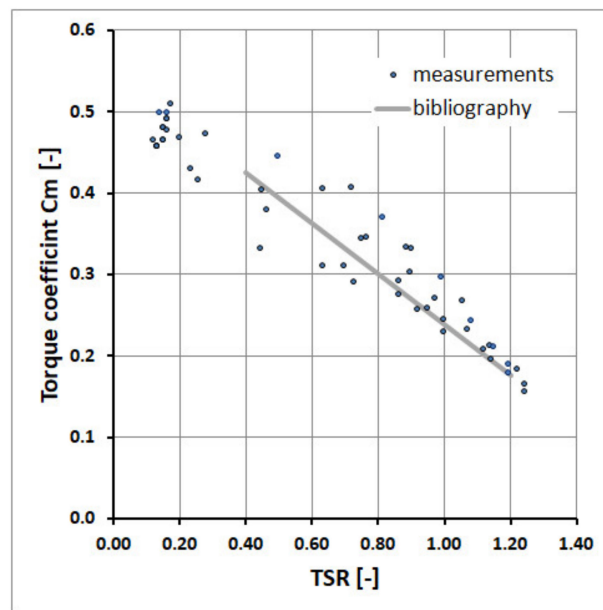


Figure 8. Torque coefficient for single-segment rotor and data from [16].

The plot in Figure 8 shows that the obtained results are close to other results found in the literature [17]. It follows from the above that placing the rotor downstream of the passage outlet is an effective method for the test stand design. Confidence can be gained that the used experimental setup may produce reliable results even in comparison with large wind tunnel measurements. This indicates that the obtained measurements are reliable in our study of a comparison between the two rotors.

#### 4.1. Single-Segment Rotor

The direct comparison of measurements on both rotors were carried out based on torque values without any normalization. Examples of measurement results at high and low wind velocities for a single-segment rotor are presented in Figure 9a,b.

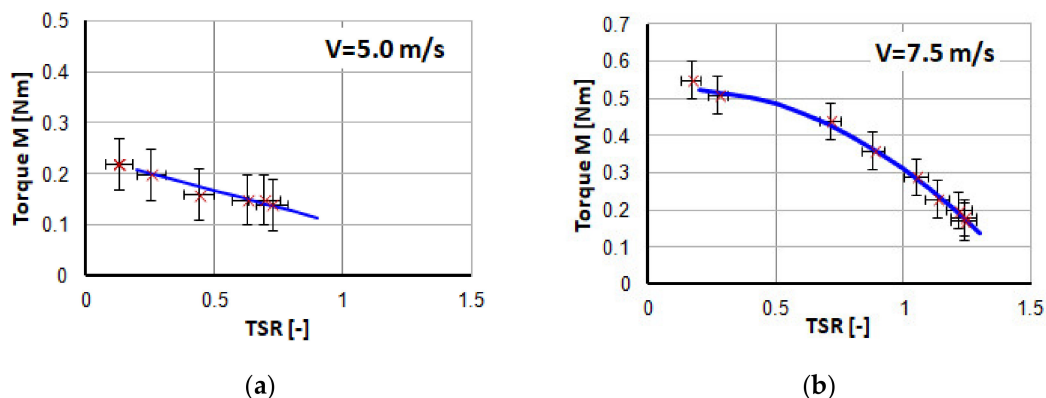


Figure 9. Torque characteristics for single-segment rotor; (a) velocity  $V = 5.0$  m/s; (b) velocity  $V = 7.5$  m/s.

The measurement points are marked by marker 'x'. The error bars are indicated (see Section 6). The characteristics of the torque may be described by the second degree polynomial function (quadratic equation) depicted as a continuous line. The type of characteristic line was chosen only because of the good quality of approximation. The

coefficients 'a', 'b' and 'c' of these approximation equations for each wind velocity case are presented in Table 1. For the lowest wind velocity the relation becomes linear.

**Table 1.** Approximation function coefficients for single-segment rotor characteristics.

V [m/s]	a1	b1	c1
7.5	−0.28	0.07	0.52
7.0	−0.24	0.04	0.47
6.5	−0.18	0.00	0.40
6.0	−0.10	−0.05	0.34
5.5	−0.04	−0.10	0.28
5.0	0	−0.14	0.24

It turns out that the dependence of these coefficients on the wind velocity may be further approximated by linear functions. This is presented in the plots in Figure 10, the error bars indicating the uncertainty of the approximation for each point are also given.

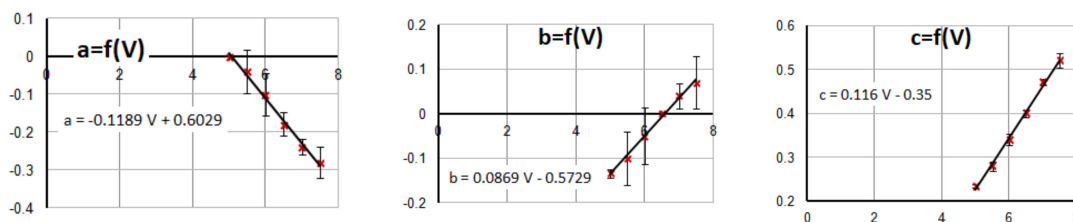


**Figure 10.** Dependence of coefficients a, b and c on wind velocity for single-segment rotor.

The approximation is linear and the coefficients may be expressed by the following equations:

$$a1 = -0.1189 \cdot V + 0.6029, \quad (4)$$

$$b1 = 0.0869 \cdot V - 0.5729, \quad (5)$$

$$c1 = 0.1160 \cdot V - 0.3500. \quad (6)$$

Hence, it follows from the above that the torque on the rotor axis  $M$  [Nm] for a single-segment rotor may be described by the function  $M = f(\text{TSR})$  with the wind velocity as a parameter  $V$  [m/s]:

$$M1 = (-0.1189 \cdot V + 0.6029) \cdot \text{TSR}^2 + (0.0869 \cdot V - 0.5729) \cdot \text{TSR} + (0.116 \cdot V - 0.35). \quad (7)$$

This relation (Equation (7)) is drawn as solid lines in the plot in Figure 11 for the indicated wind velocities. The markers represent the measurement points for each selected wind velocity. Figure 11 shows a good coincidence of the measurement points with the characteristics provided by Equation (7). The comparison scope of the measurements and Equation (7) in the TSR range from 0.2 to 1.2 and are sufficiently large for application purposes.

The above-presented torque can be expressed as a torque coefficient (Figure 12), where the dependence on the wind speed is visible. It changes the character from quadratic to linear for high velocity and low velocity, respectively. Such a presentation allows for comparison of the results with the literature. Equation (7) should not be used, however, for extrapolation to another range of wind velocities.

The analysis of the torque coefficient values creates confidence in the measurements carried out. The above approximation should not be misinterpreted with physical modeling of the Savonius rotor. This is only a method to allow a useful comparison between the two rotors within the wind velocity range from 5 m/s to 7.5 m/s for a large scope of TSR.

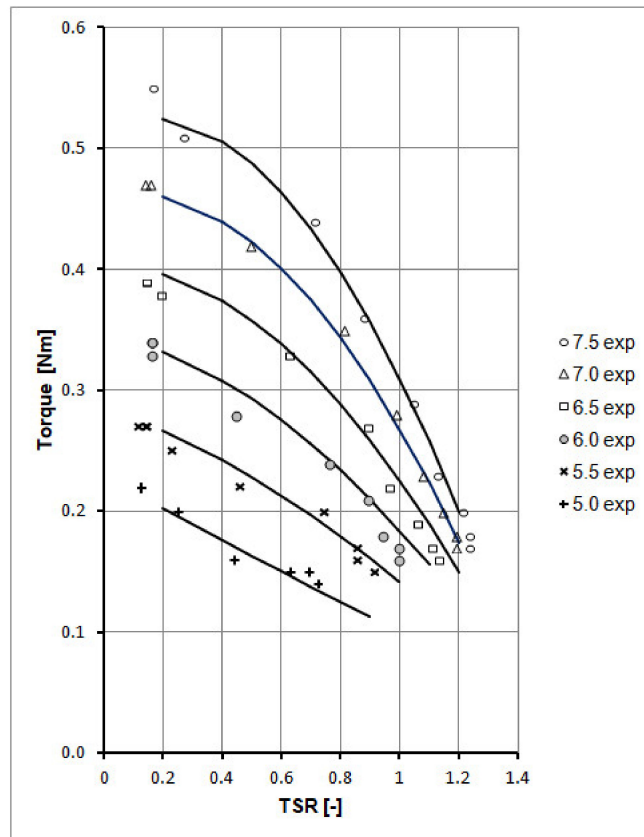


Figure 11. Comparison of measurements with approximation of characteristics (Equation (7)) for single-segment rotor.

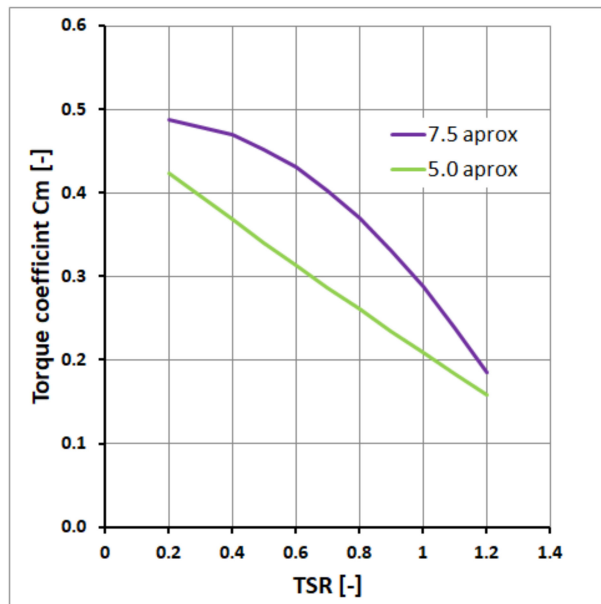


Figure 12. Approximated torque coefficient dependence on wind velocity.

#### 4.2. Four-Segment Rotor

All the measurement procedures used for the analysis of the four-segment rotor were identical, as for the single-segment rotor. The characteristic behavior of the torque  $M$  as a function of the TSR also shows the quadratic function behavior. Nonetheless, the coefficients are obviously different, as shown in Table 2.

**Table 2.** Approximation function coefficients for four-segment rotor characteristics.

V [m/s]	a4	b4	c4
7.5	−0.25	0.12	0.43
7.0	−0.20	0.07	0.38
6.5	−0.14	0.00	0.33
6.0	−0.08	−0.05	0.28
5.5	−0.03	−0.11	0.23
5.0	0.01	−0.16	0.19

The dependence of the coefficients on the wind velocity turns out also to be linear and is described by the following linear equations:

$$a4 = -0.1069 \cdot V + 0.5529, \quad (8)$$

$$b4 = 0.1137 \cdot V - 0.7324, \quad (9)$$

$$c4 = 0.0971 \cdot V - 0.3005. \quad (10)$$

Following the presented relations, an equation approximating the measured torque can be formulated in the form given by Equation (11):

$$M4 = (-0.1069 \cdot V + 0.5529) \cdot TSR^2 + (0.1137 \cdot V - 0.7324) \cdot TSR + (0.0971 \cdot V - 0.3005) \quad (11)$$

A comparison of the measurements and the approximation functions is presented in Figure 13. Different markers show the measured values for different wind velocities. The solid lines represent the approximation functions (Equation (11)) for the given wind velocity cases. The corresponding curves can be identified by the coincidence with appropriate markers.

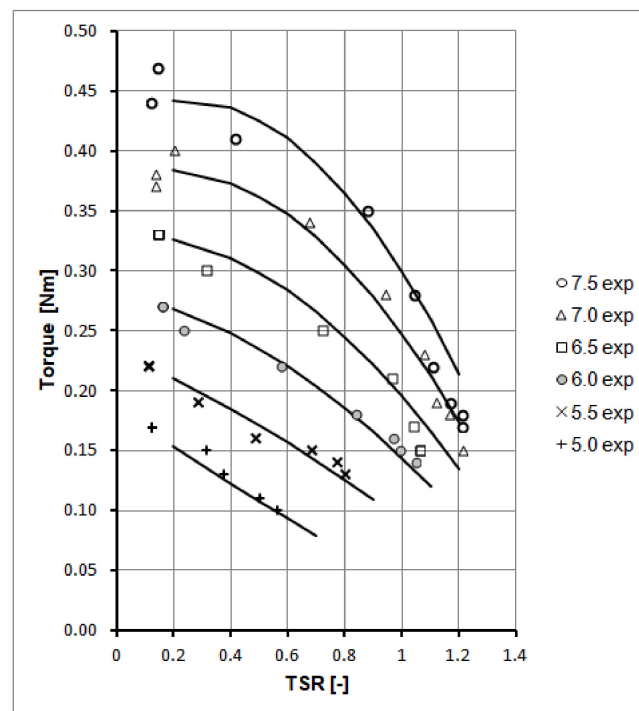


**Figure 13.** Comparison of measurements with approximation of characteristics (Equation (11)) for four-segment rotor.

The above-presented approach has shown that it is possible to provide an analytical description of the measured torque as a function of the corresponding speed coefficient

TSR for both rotors. The good coincidence of these analytical approximations with measurements gives confidence in the further comparison of the aerodynamic characteristics of these rotors.

### 5. Comparison of Characteristics of Single- and Four-Segment Rotors

A further comparison of a single-segment rotor and a four-segment rotor is carried out here on the basis of two interpolation functions of Equations (1) and (2). These provide the value of torque ( $M$ ) on the rotor axis and the rotational speed. On this basis the corresponding power delivered by the rotor can be determined from the known relation:

$$P = M \cdot \omega. \quad (12)$$

Knowing the wind velocity, the reference power of the wind stream of cross section 'A' can be calculated:

$$P_{\text{WIND}} = 0.5 \cdot \rho \cdot A \cdot V^3. \quad (13)$$

This reference power of the air stream allows the determination of the rotor power coefficient ( $C_p$ ) as:

$$C_p = P/P_{\text{WIND}}. \quad (14)$$

The obtained rotor effectiveness values should not be treated as an absolute determination of the rotor quality, which could be used for comparison with other rotors, measured by other researchers and for free wind conditions. There is a slight uncertainty as to how the reference velocity measurement point (Figure 6) is corresponding to the free wind velocity in the real conditions. Nevertheless, it is very important that both rotors are measured in the same experimental environment and with the same measurement techniques and equipment. Therefore, a comparison of the operation of these rotors is fully justified. The results presented here have to be treated as a comparative study.

It is obvious that the behavior of both rotors is dependent on the wind velocity. This is shown in Figure 14 for the maximum and minimum wind velocity in our experiment. It should be noticed that the range of  $\text{TSR} = 0.2$  to  $1.2$  is sufficient for the presented research as it includes the characteristic maximum of the power coefficient that can be obtained from the rotors of interest. The maximum effectiveness at  $V = 7.5$  m/s is nearly 30% which is within the limit for the Savonius rotor published by other research groups, as shown e.g., in [16,23]. As has been mentioned earlier, the effectiveness concerns the rotor with bearings but without an electric generator. The results are obtained in a special test section environment, not in the free wind conditions. Therefore, this high  $C_p$  value may be justified. It is worth noting that the range of the obtained power coefficients in the whole experiment spans between 0.05 to 0.3, depending on the flow conditions. This  $C_p$  range fits well with the results presented in the literature.

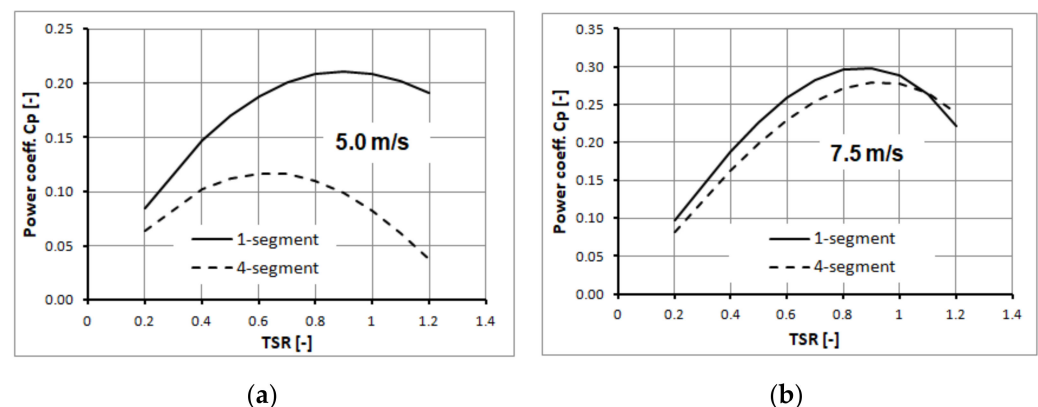


Figure 14. Comparison of rotor effectiveness ( $C_p$ ) at different TSR; (a) characteristics at 5.0 m/s; (b) characteristics at 7.5 m/s.

Figure 14 proves that the aerodynamic characteristics of both rotors nearly overlap at a high wind velocity (7.5 m/s). However, there is evident loss of effectiveness of a four-segment rotor by 10% until the maximum power is reached. This means that the introduction of segment division plates is only slightly noticeable at this wind velocity. Nonetheless, there is a small shift in the TSR for the maximum power at a 4-segment rotor towards higher values.

At lower wind velocities, the difference between the two rotors becomes considerable. The effectiveness of a 4-segment rotor is nearly two times lower than for the single-segment one. The plot for 5 m/s shows that the difference between rotors becomes very high for a high TSR and is reduced for a lower TSR case. The reduction of effectiveness is accompanied by the characteristic maximum shift to a lower TSR.

In Figure 15, the maximum effectiveness is plotted at each wind velocity. This shows clearly a higher effectiveness of the single-segment rotor in the whole range of the considered wind velocities. The difference becomes really important at low wind velocities. At higher velocities the difference becomes much smaller. Therefore, it is advisable to use single-segment rotors in the locations where the winds are low.

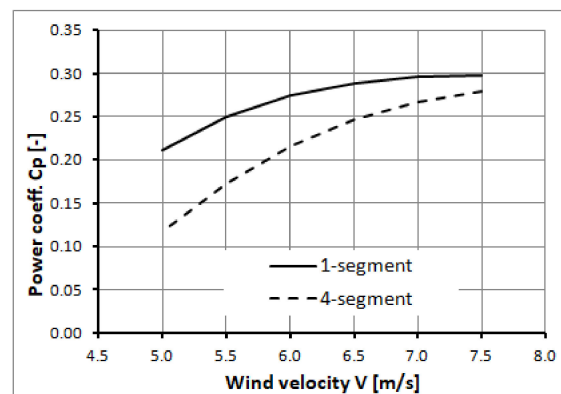


Figure 15. Maximum effectiveness ( $C_p$ ) for both rotors.

The above dependence of the rotor segmentation effect on the wind velocity is a new finding which has not been presented earlier. This observation is important from the application point of view, but the explanation of this effect is a challenge. The explanation of this effect calls for very advanced time-resolved measurements and for high fidelity unsteady numerical simulations.

It is also interesting that the maximum effectiveness for a single-segment rotor occurs always at the same value of  $TSR = 0.9$  (Figure 14). In the case of a four-segment rotor, the local maximum location shifts from  $TSR = 0.65$  at  $V = 5$  m/s up to  $TSR = 0.95$  at  $V = 7.5$  m/s. There is not enough information in the literature to generalise this result. Mostly, the maximum reported power takes place at  $TSR \approx 0.9$  and the dependence on the wind velocity is not discussed.

## 6. Uncertainty Analysis

The physical quantities measured, and thus introducing uncertainty, were: torque  $M$ , rotor circumference speed  $V_R$  involved in the calculation of the  $TSR$ , and wind velocity  $V_{WIND}$ .

A high frequency measurement of velocity for assessing the turbulence level of the test stand was done with a CTA system (DANTEC 54T30 CTA system and NI 11bit ADC working at 10 kHz). The overall uncertainty of the  $TI$  (turbulence intensity) value is lower than 10%.

The torque was measured with a torque transducer with a range of 5 Nm and with the accuracy combined with the accuracy of transmission being not lower than 2% FS at the sampling rate of 1 kHz. This introduces an average uncertainty of 15% for the cases of interest.

The circumferential speed was measured by an instrument with a reference frequency supplied by the TXCO oscillator and transmitted with an accuracy of 1 LSB (Least Significant Bit) of an 8 Bit number. The two, combined with the measurement range of the device, yield a maximum absolute error of 0.08 Hz for every measurement case.

The wind velocity (except for the turbulence level, as described above) was measured using NIST certified air velocity transducer TSI8455. The transducer range was 7.5 m/s and the absolute error introduced was 1% FS. The relative error of the wind velocity does not exceed 2% for all the cases covered in the article.

The above are summarized in Table 3.

**Table 3.** Accuracies of measurement chain elements.

Observed Value	Meter	Accuracy	Absolute Uncertainty
Torque	NCTE2000	1% FS	0.1 Nm
Torque voltage signal	External 16 bit ADC	2 LSB	Negligible
Rotational speed	$\mu$ C, TXCO based T/C	$1.0 \times 10^{-7}$	1 Hz
Wind velocity	TSI8455	2%FS	0.2 m/s
Turbulence level	CTA (DANTEC54T30)	<10%	Irrelevant

As all the above were measured with separate instruments, hence, we assume all the errors to be random and independent. For that reason, it is correct to use the simple principle of propagation of uncertainty for the product and the quotient instead of the total derivative estimation of the maximum relative error. It follows from the foregoing that, when calculating the uncertainty of power (being a product of rotational velocity  $\omega$  and torque  $M$ ) and for the TSR (being a quotient of circumferential speed  $V_R$  and wind velocity  $V_{WIND}$ ), we use the following formulas:

$$\frac{\Delta P}{P} = \sqrt{\left(\frac{\partial V_R}{V_R}\right)^2 + \left(\frac{\partial M}{M}\right)^2} \quad (15)$$

$$\frac{\Delta TSR}{TSR} = \sqrt{\left(\frac{\partial V_R}{V_R}\right)^2 + \left(\frac{\partial V_{WIND}}{V_{WIND}}\right)^2} \quad (16)$$

The magnitude of the absolute uncertainty is marked in the corresponding plots in Figure 7, but the average value of it is approximately 15% for the TSR and 20% for the torque.

The values of uncertainties are significant, but it has to be taken into account that they are accompanied by very high values of R (coefficient of determination); approximately 0.99 in most of the cases. This is essential in an analysis regarding approximations. The values of R indicate that although there is an inevitable uncertainty resulting from the apparatus, it is correct to identify the trends and approximate the torque ( $M$ ) as a quadratic function of TSR in Figure 7.

Regarding the last stage of the analysis concerning approximation of the coefficients 'a', 'b', and 'c' in Tables 1 and 2, the uncertainties were calculated from a standard linear regression analysis and they are marked in the respective plots in Figure 10.

## 7. Concluding Remarks

The main conclusions could be listed as follows:

1. The most important conclusion, new for the knowledge of Savonius rotors, is that the difference in power production between single- and four-segment rotors depends on the wind velocity;
2. The difference between these rotors increases with reduced wind velocities;
3. A single-segment rotor is more effective than a four-segment one;



4. At small wind velocities, a single-segment rotor is about 50% better than a four-segment one, with the difference in change depending on the TSR, (Figure 14a);
5. For high winds, the single-segment rotor is about 10% more effective than a four-segment one for all TSRs (Figure 14b);
6. The torque characteristics at higher velocities can be approximated by the quadratic function;
7. The torque characteristics become linear at lower wind velocities.

The main conclusion leads to a new hypothesis; that the segment dividing plates introduces effects which are dependent on the wind velocity. This could be inspiring for further investigations of these phenomena. A higher wind speed at the same TSR means the increasing rotational speed. Therefore, it can be concluded that the effect is reduced with a shorter time for rotation.

Complex vortical structures are built, developed and shaded downstream in the wake of the rotor during the rotation. These processes are time-dependent and, in shorter time, the creation of such structures is less effective. In such a case, the differences between both rotors may be strongly reduced which is proven by the presented results.

Experimental possibilities to detect the formation and development of 3-D structures, especially in the time-dependent sense, are hardly available at the moment. A detailed, high fidelity, unsteady, numerical study should be undertaken to explain the effects documented in this paper.

An important conclusion of this paper is that it is favorable to use a single-segment rotor. The presented results show that the addition of plates dividing rotor segments reduces the rotor effectiveness, which is substantial, especially at low wind velocities.

**Author Contributions:** Conceptualization, K.D.; methodology, P.D., K.D. and A.T.; software, K.D., P.D., J.T.; validation, J.T.; formal analysis, P.D., K.D.; investigation, K.D. and P.H.; resources, K.D., P.D., J.T., P.H., A.T.; data curation, K.D., J.T. and P.H.; writing—original draft preparation, P.D.; writing—review and editing, External company; visualization, K.D., P.D., P.H., J.T.; supervision, P.D., A.T.; project administration, P.D.; funding acquisition, P.D. All authors have read and agreed to the published version of the manuscript.

**Funding:** This research was funded by European Regional Development Fund, grant number POIR.04.01.04-00-0031/18-00 and by The Szewalski Institute of Fluid-Flow Machinery—Polish Academy of Sciences. The APC was funded by The Szewalski Institute of Fluid-Flow Machinery—Polish Academy of Sciences.

**Institutional Review Board Statement:** Not applicable.

**Informed Consent Statement:** Not applicable.

**Data Availability Statement:** The authors chose not to share any datasets.

**Acknowledgments:** The work was supported under the 3PioWiat project: POIR.04.01.04-00-0031/18-00, financed by the European Fund for Regional Development. Also, the work was supported by the Szewalski Institute of Fluid-Flow Machinery, Polish Academy of Sciences.

**Conflicts of Interest:** The authors declare that there is no conflict of interest. The funders had no role in the development of the study; in the collection, analyses, or interpretation of data; in the writing of the manuscript, or in the decision to publish the results.

## Nomenclature

HAWT	Horizontal Axis Wind Turbine
VAWT	Vertical Axis Wind Turbine
IMP PAN	Institute of Fluid Flow Machinery
CTA	Constant Temperature Anemometer
TXCO	Temperature Compensated Crystal Oscillator
FS	Full Scale
LSB	Least Significant Bit
$U$ [m/s]	velocity of the propelling blade with respect to the air
Re	Reynolds number based on rotor diameter



$V_{WIND}$ , $v$ , $V$ [m/s]	wind velocity
$V_R$ [m/s]	speed of the rotor circumference (at outer radius)
$M$ [Nm]	torque on the rotor axis
$M1$ [Nm]	torque for a single-segment rotor
$M4$ [Nm]	torque for a four-segment rotor
TSR [-]	tip speed ratio $\left(TSR = \frac{V_R}{V_{WIND}}\right)$
$\omega$ [1/s]	angular rotor velocity
$A$ [m <sup>2</sup> ]	rotor projection area
$Ar$ [-]	aspect ratio—segment height over rotor diameter $h/D$
$P$ [W]	power
$P_{WIND}$ [W]	power of the reference wind stream
$C_p$ [-]	power coefficient, effectiveness
$H$ [m]	rotor height
$h$ [m]	segment height
$D$ [m]	rotor diameter
$\rho$ [kg/m <sup>3</sup> ]	air density
$a1, b1, c1$	coefficients of the quadratic function for single-segment rotor
$a4, b4, c4$	coefficients of the quadratic function for four-segment rotor
ADC	Analog-to-Digital Converter
$\mu C$	microcontroller
T/C	Timer/Counter registers

## References

- Jean-Daniel, P.; Stefan, G. *Small Wind World Report by the World Wind Energy Association*; WWEA: Bonn/Monachium, Germany, 2017.
- AWEA U.S. *Market Report on U.S. Wind Technologies in Distributed Applications*; The National Technical Information Service: Alexandria, Egypt, 2012.
- Savonius, S. *The Wing-Rotor in Theory and Practice*; Savonius and Company: Helsingfors, Finland, 1926.
- Alexander, A.J.; Holownia, B.P. Wind tunnel test on a Savonius rotor. *J. Ind. Aerodyn.* **1978**, *3*, 343–351. [[CrossRef](#)]
- Fujisawa, N.; Gotoh, F. Visualization study of the flow in and around a Savonius rotor. *Exp. Fluids* **1992**, *12*, 407–412. [[CrossRef](#)]
- Saha, U.K.; Thotla, S.; Maity, D. Optimum design configuration of Savonius rotor through wind tunnel experiments. *J. Wind Eng. Ind. Aerodyn.* **2008**, *96*, 1359–1375. [[CrossRef](#)]
- Roy, S.; Saha, U.K. Review on the numerical investigations into the design and development of Savonius wind rotors. *Renew. Sustain. Energy Rev.* **2013**, *23*, 73–83. [[CrossRef](#)]
- Can, K.; Haixia, L.; Xin, Y. A Review of fluid dynamics aspects of Savonius-rotor-based vertical-axis wind rotors. *Renew. Sustain. Energy Rev.* **2014**, *33*, 499–508.
- Zemamou, M.; Aggour, M.; Toumi, A. Review of Savonius wind turbine design and performance. In Proceedings of the CPESE 2017, Berlin, Germany, 25–29 September 2017.
- Kumar, P.M.; Surya, M.R.; Narasimalu, S.; Lim, T.C. Experimental and numerical investigation of novel Savonius wind turbine. *Wind Eng.* **2019**, *43*, 247–262. [[CrossRef](#)]
- Mahmoud, N.H.; El-Haroun, A.A.; Wahba, E.; Nasef, M.H. An experimental study on improvement of Savonius rotor performance. *Alex. Eng. J.* **2012**, *51*, 19–25. [[CrossRef](#)]
- Xiaoqing, S.; Daihai, L.; Diangui, H.; Guoqing, W. Numerical study on coupling effects among multiple Savonius turbines. *J. Renew. Sustain. Energy* **2012**, *4*, 053107.
- Tahani, M.; Rabbani, A.; Kasaeian, A.; Mehrpooya, M.; Mirhosseini, M. Design and numerical investigation of Savonius wind turbine with discharge flow directing capability. *Energy* **2017**, *130*, 327–338. [[CrossRef](#)]
- Driss, Z.; Mlayeh, O.; Driss, D.; Maaloul, M.; Abid, M.S. Numerical simulation and experimental validation of the turbulent flow around a small incurved Savonius wind rotor. *Energy* **2014**, *74*, 506–517. [[CrossRef](#)]
- Kacprzak, K.; Liskiewicz, G.; Sobczak, K. Numerical investigation of conventional and modified Savonius wind turbines. *Renew. Energy* **2013**, *60*, 578–585. [[CrossRef](#)]
- Kamoji, M.A.; Kedare, S.B.; Prabhu, S.V. Experimental investigations on single stage modified Savonius rotor. *Appl. Energy* **2009**, *86*, 1064–1073, ISSN 0306-2619. [[CrossRef](#)]
- Blackwell, B.F.; Sheldahl, R.E.; Feltz, L.V. *Wind Tunnel Performance Data for Two-And Three-Bucket Savonius Rotors*; SAND76-0131; Sandia Laboratories: Albuquerque, NM, USA, 1978.
- Akwa, J.V.; da Silva, G.A., Jr.; Petry, A.P. Discussion on the verification of the overlap ratio influence on performance coefficients of a Savonius wind rotor using computational fluid dynamics. *Renew. Energy* **2012**, *38*, 141–149. [[CrossRef](#)]

19. Hercul, P. Tree-Dimensional Flow Structures Effect on the Savonius Rotor Efficiency. Master's Thesis, Gdańsk University of Technology, Gdańsk, Poland, 2018. (In Polish).
20. Sharma, S.; Sharma, R.K. Performance improvement of Savonius rotor using multiple quarter blades—A CFD investigation. *Energy Convers. Manag.* **2016**, *127*, 43–54. [[CrossRef](#)]
21. Jaohindy, P.; McTavish, S.; Garde, F.; Bastide, A. An analysis of the transient forces acting on Savonius rotors with different aspect ratios. *Renew. Energy* **2013**, *55*, 286–295. [[CrossRef](#)]
22. Akwa, J.V.; Vielmo, H.A.; Petry, A.P. A review on the performance of Savonius wind turbines. *Renew. Sustain. Energy Rev.* **2012**, *16*, 3054–3064. [[CrossRef](#)]
23. Sobczak, K. Numerical investigations of an influence of the aspect ratio on the Savonius rotor performance. In *Journal of Physics: Conference Series, Proceedings of the XXIII Fluid Mechanics Conference (KKMP 2018), Zawiercie, Poland, 9–12 September 2018*; IOP Publishing: Bristol, UK, 2018; Volume 1101, p. 012034.
24. Doerffer, P.; Doerffer, K.; Ochrymiuk, T.; Telega, J. Variable Size Twin-Rotor Wind Turbine. *Energies* **2019**, *12*, 2543. [[CrossRef](#)]
25. Luczak, M.; Telega, J.; Zagato, N.; Mucchi, E. On the damage detection of a laboratory scale model of a tripod supporting structure by vibration-based methods. *Mar. Struct.* **2019**, *64*, 146–160. [[CrossRef](#)]
26. Damak, A.; Driss, Z.; Abid, M.S. Optimization of the helical Savonius rotor through wind tunnel experiments. *J. Wind Eng. Ind. Aerodyn.* **2018**, *174*, 80–93. [[CrossRef](#)]
27. Shigetomi, A.; Murai, Y.; Tasaka, Y.; Takeda, Y. Interactive flow field around two Savonius turbines. *Renew. Energy* **2011**, *36*, 536–545. [[CrossRef](#)]
28. Doerffer, K. Investigations and Development of Innovative Wind Power Plant. Ph.D. Thesis, Faculty of Mechanical Engineering, UTP, Bydgoszcz, Poland, 2019. (In Polish).
29. Menet, J.-L. A double-step Savonius rotor for local production of electricity: A design study. *Renew. Energy* **2004**, *29*, 1843–1862. [[CrossRef](#)]
30. Jian, C.; Kumbernuss, J.; Linhua, Z.; Lin, L.; Hongxing, Y. Influence of Phase-Shift and Overlap Ratio on Savonius Wind Turbine's Performance. *J. Sol. Energy Eng.* **2012**, *134*, 011016. [[CrossRef](#)]
31. Hayashi, T.; Li, Y.; Hara, Y.; Suzuki, K. Wind Tunnel Tests on a Three-stage Out-phase Savonius Rotor. *JSME Int. J. Ser. B* **2004**, *48*, 2005.
32. Roy, S.; Ducoin, A. Unsteady analysis on the instantaneous forces and moment arms acting on a novel Savonius-style wind turbine. *Energy Convers. Manag.* **2016**, *121*, 281–296. [[CrossRef](#)]
33. Bardala, L.M.; Sætrana, L.R. Influence of turbulence intensity on wind turbine power curves. In *Proceedings of the 14th Deep Sea Offshore Wind R&D Conference, EERA DeepWind'2017, Trondheim, Norway, 18–20 January 2017*.
34. Hedevang, E. Wind turbine power curves incorporating turbulence intensity. *Wind Energy* **2014**, *17*, 173–195. [[CrossRef](#)]

